Earth and Planetary Science Letters 604 (2023) 117991

Contents lists available at ScienceDirect

Earth and Planetary Science Letters

journal homepage: www.elsevier.com/locate/epsl

Cenozoic topographic evolution of the Southern Central Andes foreland as revealed by hydrogen stable isotopes in hydrated volcanic glass

Lucas M. Fennell [a,b,*], Mark T. Brandon [b], Michael T. Hren [c]

[a] CONICET - Universidad de Buenos Aires, Instituto de Estudios Andinos Don Pablo Groeber (IDEAN), Intendente Güiraldes 2160, Pabellón II, 1428, Buenos Aires, Argentina
[b] Department of Earth and Planetary Sciences, Yale University, New Haven, CT, USA
[c] Department of Earth Sciences, University of Connecticut, Storrs, CT, USA

ARTICLE INFO

Article history:
Received 20 March 2022
Received in revised form 16 September 2022
Accepted 5 January 2023
Available online xxxx
Editor: A. Webb

Keywords:
paleotopography
Andes
stable isotopes
volcanic glass
orographic precipitation
dynamic topography

ABSTRACT

We use the "isotope-paleotopography" method to resolve the topographic evolution of the Southern Central Andes and adjacent foreland to the east, at the latitude of 35°S. Our analysis is based on δ^2H measurements from hydrated volcanic glass from 107 samples collected from a 55 to 10 Ma stratigraphic section in the Malargüe basin, and from an additional 11 samples of Quaternary tuffs. The results are supported by an analysis of a large dataset of modern meteoric water samples ($n = 197$), which are used to characterize the relationship between orographic lifting and precipitation isotopes in the modern. Our interpretations are guided by the Orographic Precipitation and Isotopes (OPI) programs, which provide a full simulation of the flow of moist air over a specified 3D topography and the resulting condensation and fall out of rain and snow, and the isotopic fractionation associated with these processes. The OPI model is fit, in a least-squares sense, to the modern isotope data, which provides a way to test for moisture sources and to calculate how precipitation isotopes would be influenced by variations in climate.

There are three important conclusions from these data: 1) OPI modeling of modern water isotopes shows that precipitation at the Malargüe study area is derived solely from the moist northeasterly winds. The isotopic fractionation along this wind path occurs by lifting over the Córdoba and San Luis basement highs, and during the initial rise up the east side of the range. Westerly moist air is able to pass over the range, but downslope flow over the east side means that this source becomes strongly undersaturated, so precipitation from this source is suppressed in this area. 2) Our volcanic glass data indicate that the hydrogen isotopic composition of precipitation, δ^2H, has been strongly depleted, by −50 to −90 per mil, since 55 Ma to present. The only way to produce this depletion is by upslope flow of moist winds and associated precipitation over the eastern side of the range. The amount of isotopic fractionation remains fairly constant and similar to modern for the interval from 55 to 15 Ma, which indicates that the topography to the east of Malargüe has been fairly steady during that time interval. 3) Our δ^2H record indicates that between 15 and 10 Ma, the topography upwind of Malargüe decreased by about 50%, and then increased by the same amount between 10 and 0 Ma. This subsidence event coincides with the Paranense marine transgression, and is also predicted by numerical modeling of mantle flow and dynamic topography associated with subduction of the Nazca plate.

1. Introduction

The Andes have served as a natural laboratory for the study of the interplay between plate subduction, arc magmatism, mountain-building, climate change, and basin analysis (Allmendinger, 1986; Kay and Mahlburg-Kay, 1991; Ramos, 1999; Strecker et al., 2007; Horton, 2018). The topographic evolution of the Andes has traditionally been interpreted in terms of the timing of thrust faulting, and the generation and transport of syn-orogenic sediments. New methods from thermochronology, geomorphology and isotope paleotopography have started to expand our understanding of the evolution of topography and interplay between uplift, climate and erosion. Numerical modeling of subduction and mantle flow has highlighted the importance of changing dynamic topography across the Andes (Dávila et al., 2010; Flament et al., 2015).

* Corresponding author at: CONICET - Universidad de Buenos Aires, Instituto de Estudios Andinos Don Pablo Groeber (IDEAN), Intendente Güiraldes 2160, Pabellón II, 1428, Buenos Aires, Argentina.
E-mail address: lucasfennell90@gmail.com (L.M. Fennell).

https://doi.org/10.1016/j.epsl.2023.117991
0012-821X/

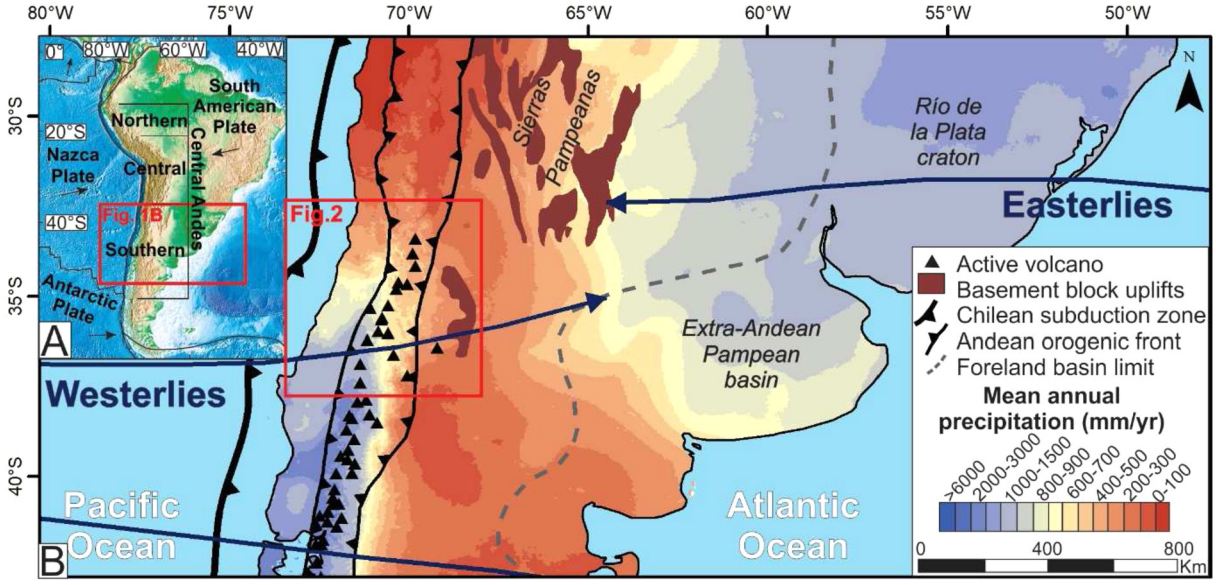

Fig. 1. A) Tectonic framework of South America and subdivision of the Andes based on Ramos (1999). B) Main tectonic features of the Southern Central Andes and eastern foreland region (based on Folguera and Zárate, 2019 and Horton, 2018) with superposed mean annual precipitation map (based on data from Fick and Hijmans, 2017) and arrows representing the principal wind circulation patterns in this area (taken from Blisniuk and Stern, 2005).

Our study focuses on the use of the hydrogen stable isotopes to directly measure the evolution of topography across the Andes. This approach is based on the *altitude effect* observed in precipitation isotopes (Dansgaard, 1964). This effect describes the common observation that the stable isotope composition of hydrogen and oxygen in precipitation tends to have a strong linear correlation with elevation of the sample. Ambach et al. (1968) provides an early example of this linear relation, as shown by the isotopic composition of precipitation and glacial ice as a function of elevation along modern glaciers in the Alps. This empirical relationship has been widely used for almost three decades now to study the topographic evolution of mountain ranges over geologic time (Drummond et al., 1993; Norris et al., 1999; Garzione et al., 2000; Poage and Chamberlain, 2001; Rowley et al., 2001; Blisniuk and Stern, 2005; Rowley and Garzione, 2007). Norris et al. (1999) coined the term "isotope paleoaltimetry". We prefer the term "isotope paleotopography" given that isotopic fractionation occurs as moist air moves across the topography, and thus the amount of fractionation is only loosely linked to the elevation where the precipitation reaches the Earth's surface.

A key aspect of our study is the use of hydrated volcanic glass from fine-grained clastic rocks. Previous studies have focused on hydrated glass from volcanic tuffs, but we have found that fine-grained glass is common in sediments east of the Andes (Colwyn et al., 2019). The advantages are that glass grains are small enough to ensure full hydration and that samples can be collected throughout a sedimentary sequence, which allows high sampling density.

Glass provides a robust sample of the hydrogen isotopes from meteoric water surrounding the sediment after deposition. Volcanic glass has low water content immediately after formation but the glass hydrates in the surface environment over a period of 1 to 10 ka (Friedman et al., 1993a, 1993b; Cerling et al., 1985). Friedman et al. (1993a, 1993b) show that this process of hydration is characterized by a consistent isotopic fractionation, enabling reconstruction of paleowater isotopes from δ^2H of volcanic glass (δ^2H_{glass}). Upon hydration (typically several wt% of meteoric water), hydrogen exchange becomes negligible, and its isotopic values appear to be resistant to diagenetic alteration (Colwyn et al., 2019; Cassel and Breecker, 2017). Our study finds that volcanic glass is commonly preserved in sediments going back to 55 Ma, and perhaps longer. The presence of the glass is expected given that the Andean magmatic arc has been a continuous feature in the study area throughout the Cenozoic (Litvak et al., 2019).

We collected 111 paleosol and fluvial sediments from the Malargüe basin (~35°S), which was formed in the foreland east of the Southern Central Andes (SCA) (Fig. 1). Volcanic glass was separated from 107 of these samples and analyzed for δ^2H. This record is unusual in that it is long (55 to 10 Ma), and densely sampled (sampling interval equals ~0.4 Ma). These factors help assess the fidelity of the record and resolve the influence of topography and climate. In addition, we collected samples of Quaternary tuffs across the range and modern river waters from the foreland between 32° and 38°S. The tuffs were analyzed for δ^2H, and the waters for δ^2H and $\delta^{18}O$. The modern water samples are used to evaluate moisture sources and the relationship between orographic lifting, climate, and isotopic fractionation.

2. Stratigraphy, age control and sampling of the Malargüe basin

The Malargüe basin originated as a foreland sequence on the east side of the SCA and was accreted into the SCA thrust belt at ~5 Ma (Fig. 2). At a broader scale, the SCA is a long-lived thrust belt and contains a series of east- and west-verging thrust belts and an active magmatic arc (Farías et al., 2010). In the vicinity of Malargüe, the topography of the SCA has a mean elevation of 3-4 km and peaks in excess of 5 km. Farther east of the Malargüe thrust slice is the thrust-bounded basement slice of the San Rafael block (Ramos et al., 2014). Foreland basin sediments extend 800 km east of the orogenic front and are interrupted by a forebulge high located ~300-500 km from the orogenic front (Folguera and Zárate, 2019).

2.1. Stratigraphy of the Malargüe basin

The Malargüe basin contains Late Cretaceous to Neogene terrestrial sediments derived mainly from the high Andes, and only briefly interrupted by a latest Cretaceous marine transgression (Combina and Nullo, 2011; Horton et al., 2016). The Cenozoic part of the basin starts with the Paleocene to middle Eocene Pircala

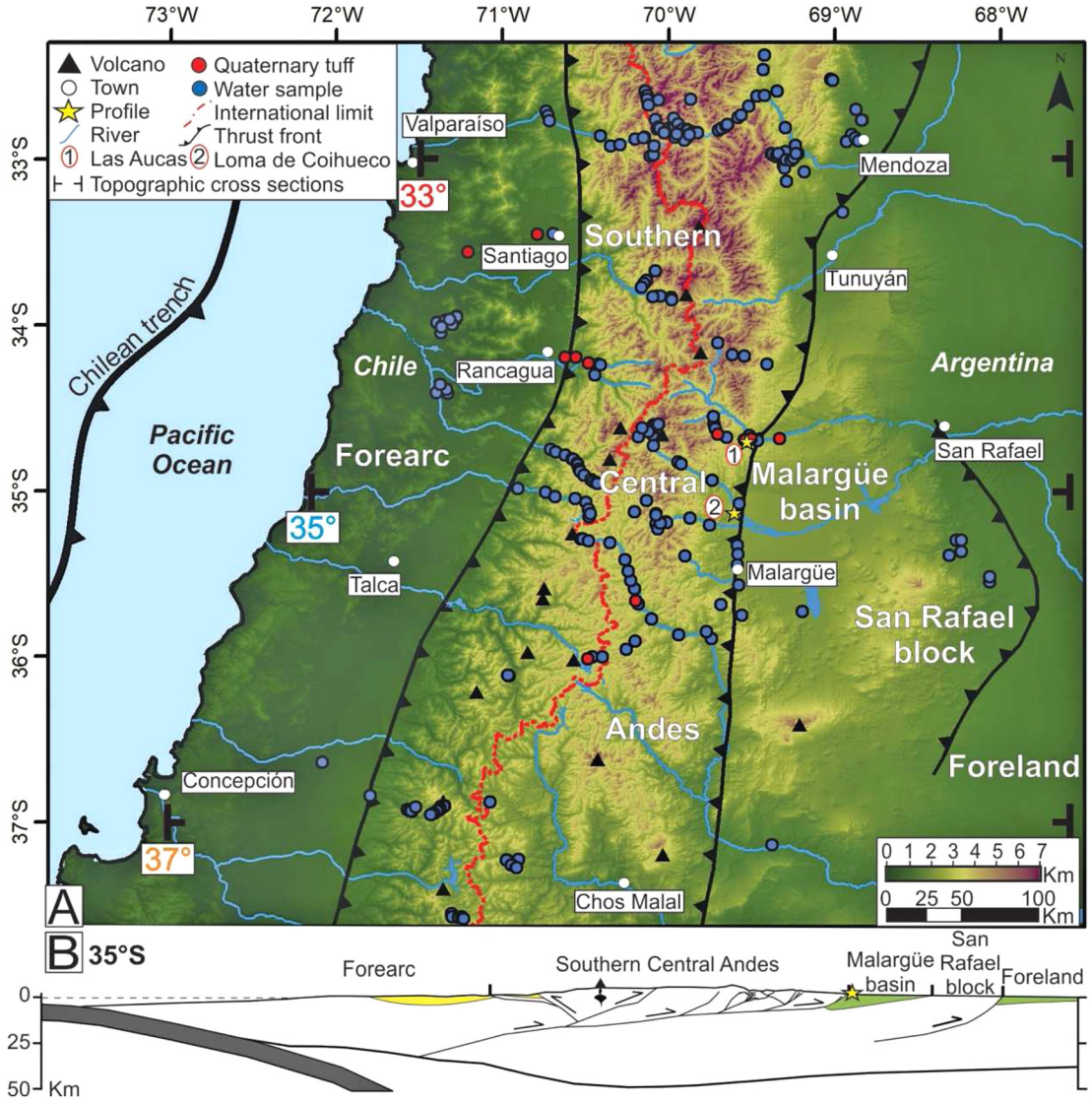

Fig. 2. A) Topographic map showing the main tectonic units of the study area, along with the localities mentioned in the text and the location of the modern tuffs, water samples, and stratigraphic profiles surveyed in the Malargüe basin. B) Cross section of the study area at 35°S showing the location of the Malargüe basin between the Southern Central Andes and the San Rafael block (modified from Horton, 2018).

Formation, consisting of mudstones and fine-grained sandstones, and volcanic tuffs (Horton et al., 2016; Horton and Fuentes, 2016). This unit is followed by the middle to late Eocene Coihueco Formation, which is comprised mainly of mudstones and isolated sandstone channels (Horton et al., 2016; Horton and Fuentes, 2016). The next highest unit is the Rodados Lustrosos, a conglomeratic and muddy unit, with distinctive polished pebbles and small cobbles. The cobbles are heavily oxidized and covered with desert varnish, which may indicate slow deposition (Combina and Nullo, 2011; Garrido et al., 2012; Horton et al., 2016). There are two proposed ages for this unit: late Eocene – early Oligocene following Garrido et al. (2012) or late Eocene – early Miocene according to Horton et al. (2016). In addition, Horton et al. (2016), and Horton and Fuentes (2016) argue that this interval has a stratigraphic break between 40 to 20 Ma. Our work in the Malargüe area indicates that the ~160 m interval between dated horizons is composed of relatively uniform fine-grained sediments (Figs. S1, S2 and S3). We found no direct evidence of a stratigraphic break. Our interpretation is that deposition rates were low during this interval (Fig. S4). As such, we assign samples ages across this interval by assuming a constant sedimentation rate, as indicated by the ages for the dated horizons that bound the interval.

The upper part of the Rodados Lustrosos, and early and middle Miocene Agua de la Piedra Formation show upward coarsening (Combina and Nullo, 2011; Horton et al., 2016; Horton and Fuentes, 2016). The Agua de la Piedra formation contains sandstone, mudstone, and conglomerate. The middle to late Miocene Loma Fiera Formation shows a greater proportion of volcaniclastic and gravel-rich sediments (Combina and Nullo, 2011; Horton et al., 2016; Horton and Fuentes, 2016). The highest preserved unit in the Malargüe basin is the late Miocene coarse-grained Tristeza Formation. This last unit provides a lower constraint for the timing of imbrication and accretion of the Malargüe section and basement rocks of the San Rafael block into the SCA thrust belt. Geologic constraints indicate that this accretion was completed by the Pliocene (Ramos et al., 2014; Horton et al., 2016).

2.2. Sampling and age control

Our sampling was done in a composite section consisting of two stratigraphically overlapping sequences (Fig. 3). The age con-

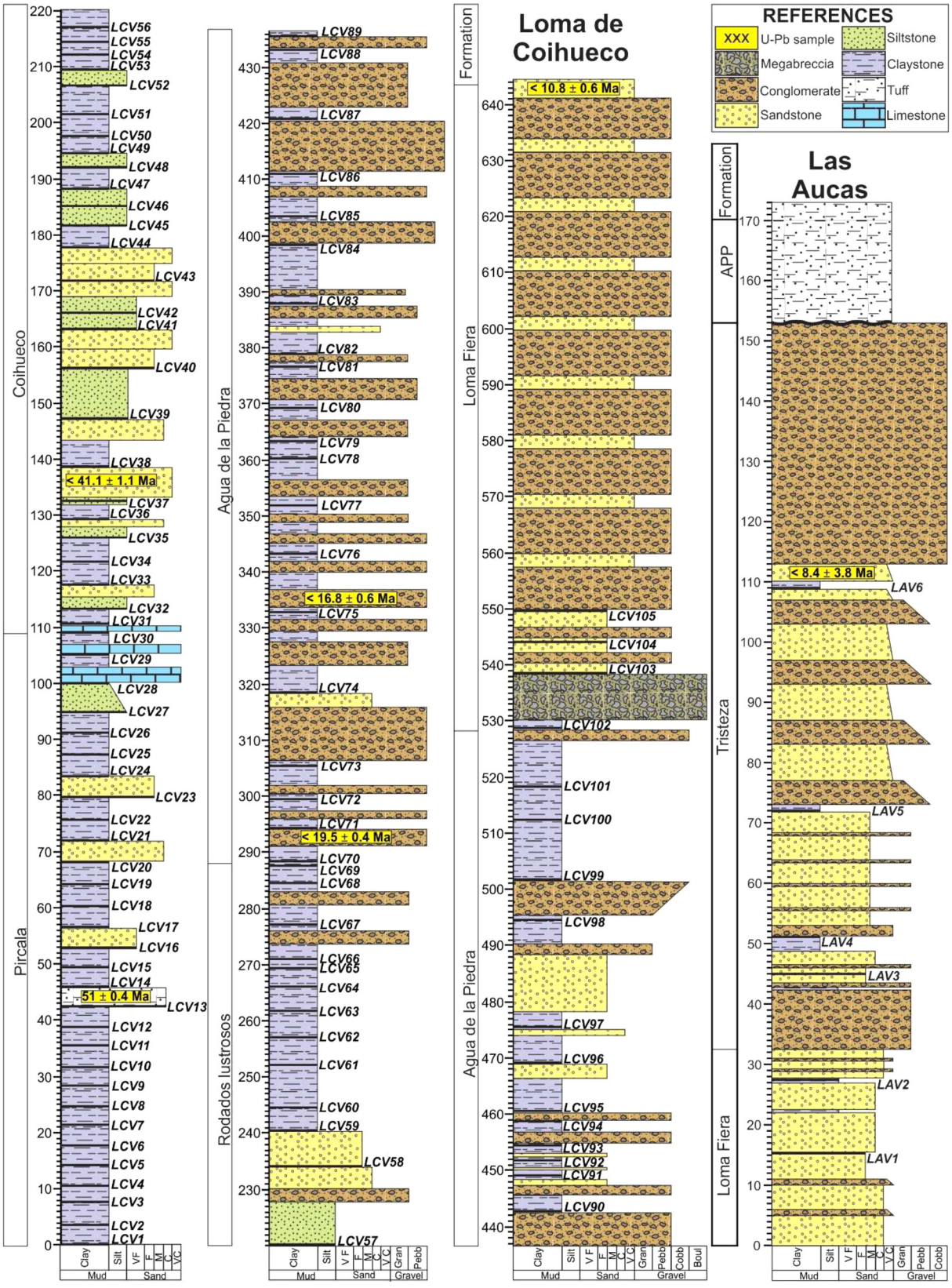

Fig. 3. Stratigraphic sections with sample locations (black horizontal bars) and U-Pb ages obtained from Horton et al. (2016) for Loma de Coihueco and Horton and Fuentes (2016) for Las Aucas. Location of the stratigraphic profiles is shown in Fig. 2A.

trol for the stratigraphic sequences is given by 5 U-Pb detrital zircon samples and by 1 U-Pb zircon crystallization age (Horton et al., 2016; Horton and Fuentes, 2016). The older sequence is located to the south at Loma de Coihueco (equivalent to profile 1 of Horton et al., 2016) and the younger (Las Aucas) lies ~50 km to the north (Fig. 2A).

Arc magmatism was active through the Cenozoic to the west of the Malargüe basin. All of the Malargüe sediments contain abundant volcanic detritus. Thus, we infer that the youngest age fraction in each detrital zircon sample is equal to the depositional age of the sample. This interpretation is consistent with stratigraphic correlations within the basin, and with available fossil ages and radiometric ages for interbedded volcanic rocks.

Within our sampled section, age is determined by interpolation between well-dated control points and extrapolation for the upper and lower parts of the section (Table S1). The upper age constraint for the Las Aucas profile was obtained from a zircon U-Pb maximum depositional age of a sandstone located immediately below a continuous 40-meter-thick conglomeratic horizon in the Agua del Médano locality (Combina and Nullo, 1997; Horton et al., 2016), which can be traced back to the Las Aucas section 5 km to the west (Fig. 2). The age of the late Miocene coarse-grained Tristeza Formation is constrained by two samples of detrital zircon U-Pb ages (Horton et al., 2016; Horton and Fuentes, 2016).

We collected 105 samples from the lower sequence (Loma de Coihueco), which is 645 m long and spans the Pircala, Coihueco, Rodados Lustrosos, Agua de la Piedra and Loma Fiera formations (Fig. 3). Nearly all samples contained abundant volcanic glass. The upper sequence was surveyed in the locality of Las Aucas to extend our analysis into the late Miocene and provide a link to Quaternary glass outcrops, which sit unconformably on top of the stratigraphic section (Fig. 3). The middle to late Miocene units contain lenses of mudstones and fine-grained sandstones interbedded with thick and massive conglomeratic strata. We were only able to collect 6 fine-grained samples along this 153-meter section. Combina and Nullo (1997) report two stratigraphic profiles, one from Las Aucas and one 5 km to the east, in Agua del Médano. They assigned a middle – late Miocene age to this unit. Recent U-Pb detrital zircon ages support this age (Horton and Fuentes, 2016) and indicate that these deposits are part of the Tristeza Formation (Fig. 3).

In addition, we collected Quaternary tuffs which are related to a series of eruptions with deposits extending from the Pacific coast, across the range, and into the Malargüe basin (Stern et al., 1984; Hildreth et al., 1984, 2009). These samples are used to assess modern relationships between glass isotopes and elevation on both eastern and western flanks of the SCA (Fig. 2A) (Table S1).

2.3. Separation and isotopic analyses of glass

Volcanic glass was separated at Yale University using methods described in Colwyn et al. (2019). Approximately 250 grams of rock were crushed with mortar and pestle, and dry-sieved to isolate the 180 to 63 μm fraction. Clay and carbonate were then removed by a series of rinses with deionized water, sodium pyrophosphate deflocculant solution, and 10 percent HCl. Magnetic grains were removed through a series of runs using a Frantz Isodynamic magnetic separator. A density separation using heavy liquids (lithium polytungstate solution, 2.48 g/cm^3) was performed to separate glass (typically 2.3-2.4 g/cm^3) from silicates such as feldspar and quartz (>2.6 g/cm^3). Resulting splits were inspected using a microscope, to ensure clean separates of glass shards, which were then stored in a glass desiccator for one week prior to analysis. These were weighed into silver capsules, dried in a vacuum oven for ~24 hours at 80 °C, and flushed with He gas. The δ^2H_{glass} was measured using a thermal conversion elemental analyzer (TC/EA) attached to a Thermo MAT 253 IRMS at the University of Connecticut. Isotopic compositions were determined relative to repeated runs of standard materials: PEF-1 (foil), NBS-22 (oil), and KGa-1 (kaolinite). The fractionation factor of Friedman et al. (1993a) was used to convert the measured δ^2H_{glass} to the δ^2H of the water associated with hydration. Water contents were determined by the TC/EA, and had an average value of 5 weight percent, which is typical for environmentally hydrated glasses (Table S1 and Fig. S5).

A set of 5 glass separates were imaged using an SEM and analyzed using an attached EDX system. The SEM images (Fig. 4) and EDX analyses of glass separates from Malargüe basin sediments confirm that these are pristine volcanic glass with minimal or no secondary mineral coatings and/or clays. About a third of the grains show evidence of pumaceous textures. The EDX system was used to acquire 33 spot analyses (Figs. S6, S7, S8, S9 and S10). The SiO_2, Al_2O_3, and CaO concentrations are consistent with volcanic compositions ranging from andesite to rhyolite. A few of the spot measurements show nearly pure SiO_2, which may indicate the presence of modal quartz.

Our measurements of the δ^2H_{glass} are based on the average of about 1 to 5 replicates per sample, depending on the amount of available material (Table S1). We use replicate measurements to determine a pooled standard deviation, s_p, for the full data set. The standard error for each sample is then given by $SE_i = s_p/\sqrt{n_i}$. And, as expected, $SE_i = s_p$ when $n_i = 1$. The accepted formula for the pooled standard deviation is $s_p = \sum_{i=1}^{m}(n_i - 1)s_i^2 / \sum_{i=1}^{m}(n_i - 1)$, where $i = 1$ to m samples in the dataset, s_i is the sample standard deviation, and n_i is the number of replicates for the ith sample (Upton, 2008). For our dataset, s_p is equal to 6.33‰.

3. Results

3.1. Modern isotopic climatology

We use 197 water isotope values that represent primary meteoric water (unaffected by post-precipitation evaporation), generally from small catchments and collected during baseflow to ensure long residence time, to characterize the relationship between isotopic composition, topography and orographic precipitation. These data are part of a larger compilation (589 unique samples) of water isotopes collected across a ~365 × 575 km region surrounding Malargüe (Fig. 2A) (Brandon et al., 2022b).

Fig. 5 shows the distributions of water δ^2H in three sections across the range. There is a clear isotopic depletion that occurs with increasing elevation on both sides of the range (Fig. 5). Upslope flow of moist wind is required to produce a negative isotopic gradient. The presence of two gradients on both west and east sides of the Andes indicates two wind sources. The precipitation that falls on the west flank is due to upslope lifting of winds coming off the Pacific Ocean, and the precipitation that falls on the east flank is due to winds from the Atlantic Ocean. It is also important to note that the estimates of δ^2H of water provided by Quaternary tuffs match those for the modern meteoric waters (Fig. 5).

We use the Orographic Precipitation and Isotope (OPI) programs of Brandon (2022) to analyze the 197 primary samples from our Malargüe study area. The OPI programs provide a full representation of the steady flow of moist air over an arbitrary 3D topography, and the down-wind evolution of cloud water, precipitation, and stable isotope concentrations associated with that flow. The catchment region is calculated for each sample, and used to integrate the precipitation and precipitation isotopes captured by the catchment.

The OPI programs include the capability to find a least-squares fit of the meteoric water isotope data relative to the model, and a best-fit estimate of a set of OPI parameters. A “one-wind” solution is defined by nine parameters: mean wind speed U, mean wind

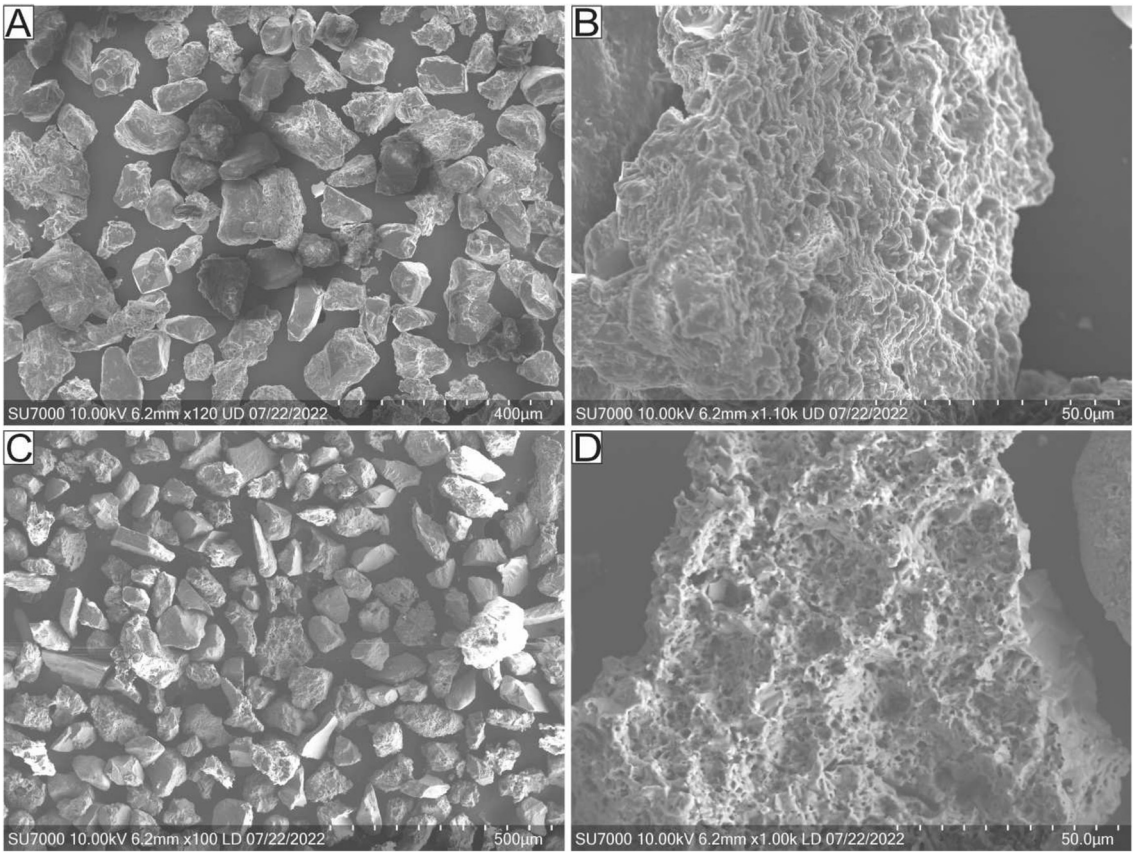

Fig. 4. SEM images of glass separates obtained from sedimentary samples show primary pumiceous textures, sharp edges, and concave fractures. A) LAV3, obtained from a sandstone. B) Zoom of central grain in A. C) LAV5, separated from a claystone. D) Zoom of central shard in C.

direction *azimuth*, sea-level surface-air temperature T_0, mountain-height number M, horizontal eddy diffusivity κ, mean residence time for cloud water τ_c, the hydrogen isotopic composition of base precipitation at the centroid of the sample data δ^2H_0, the latitudinal gradient of hydrogen isotopic composition of base precipitation $d(\delta^2H)$ / d(latitude), and the fraction of precipitation remaining after evaporation f_p. Our study here uses a "two-wind" solution, which is defined by a set of nineteen parameters. This set is simply a mixture of two "one-wind" solutions (9 parameters $\times$ 2) plus an addition parameter that describes the proportion of the total precipitation field that is associated with the first "one-wind" solution.

Brandon (2022) and Brandon et al. (2022a, 2022b) are available as open access at Github and Zenodo repository. Brandon (2022) includes a full and open distribution of the OPI programs, which are written in MATLAB, and include a description of the design and operation of the programs, and the definition of parameters and terminology, and a synthetic example of orographic precipitation associated with moist air flowing over a Gaussian-shaped mountain range. Brandon et al. (2022a, 2022b) report OPI results for the analysis of two large water-isotope datasets, one from the Patagonian Andes, and the other from the SCA dataset considered here. Both reports include all of the input data, the output from the OPI programs, and a summary of the main results.

The OPI programs are also used to estimate the influence of climate on the isotopic fractionation associated with orographic precipitation in the past. We discuss this method in association with our interpretation of the glass isotope data.

We conducted about 55 runs to test and confirm the best-fit OPI solution for the SCA isotope data. The runs clearly indicate that the isotope data are best-fit by a "two-winds" solution, with one moist wind out of the northeast and the other out of the west (see Fig. 6 for precipitation maps for each source). The northeasterly wind source carries moisture from the Atlantic and flows over the southern Sierras Pampeanas, the foreland, and the SCA. Fig. 6a shows that orographic precipitation from this source occurs on northeast-facing topographic slopes because the airflow is upslope in those areas. In contrast, the southeast-facing slopes are dry. Precipitation rates are largest over the basement uplifts of the southern Sierras Pampeanas and the east flank of the SCA, but this source also produces local precipitation in Chile as well (38°S, 73°W).

The westerly wind source carries moisture from the Pacific and flows over the Coastal Cordillera of Chile and the SCA. Upslope flow and orographic precipitation occurs on west-facing slopes, and east-facing slopes are dry. The largest precipitation rates are on the west slope of the SCA, but note that this precipitation is created in scattered locations to the east of the SCA, and these locations correspond to the western slopes of smaller topographic highs in that region.

These relationships should make it clear that both wind sources are able to cross the SCA, so topographic blocking is not an issue. This point is also clearly demonstrated by the best-fit estimates of the mountain-height number for each wind source (see Brandon et al., 2022b for details). The precipitation pattern might be viewed as evidence of blocking, but the dry aspect of the leeward slopes is due to the fact that as the air flows downslope, a parcel of air that moves with that flow becomes undersaturated. This is not due to loss of moisture but rather due to the increase in pressure and temperature as the parcel moves downward within the atmosphere. Our OPI modeling shows that downslope flow of the westerly wind source over the east side of the SCA strongly suppresses westerly-derived precipitation from forming or falling in that region. As a result, the orographic precipitation that falls

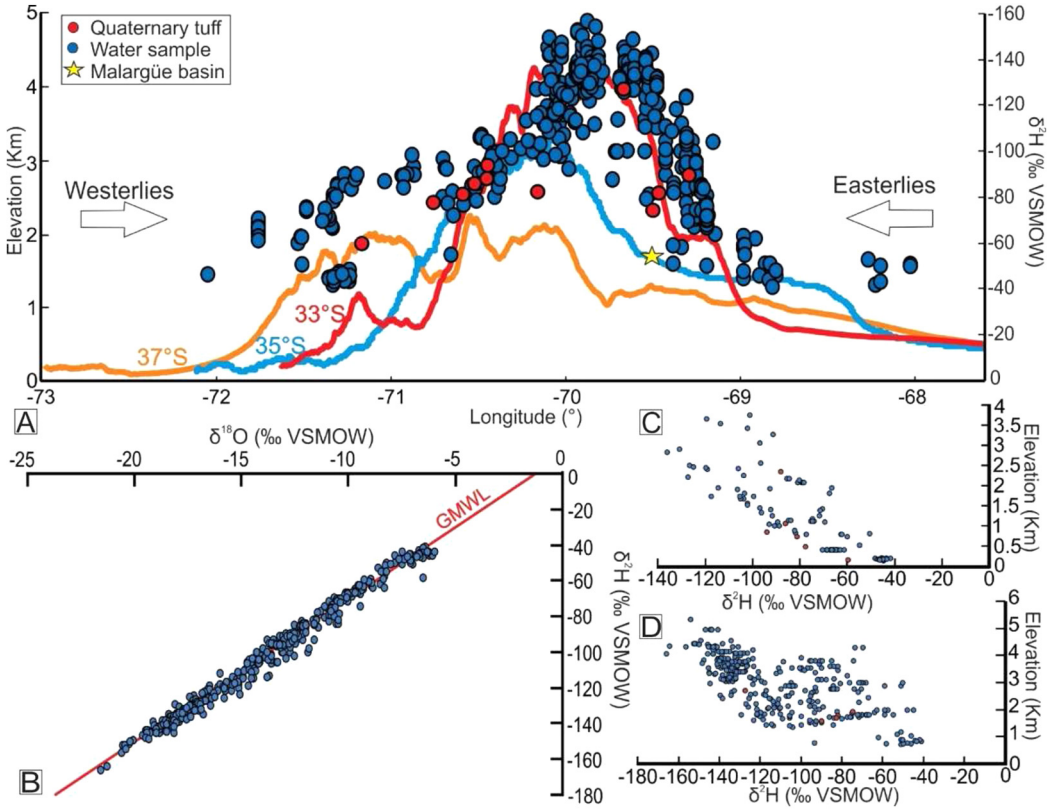

Fig. 5. A) Mean topography at 33°S, 35°S and 37°S (location of the cross sections in Fig. 2A), modern water δ^2H (taken from the dataset presented in Brandon et al., 2022b, excluding trunk rivers and precipitation samples) and δ^2H_{glass} values from Quaternary tuffs converted to meteoric water composition (Friedman et al., 1993a). B) Plot of δ^2H vs. $\delta^{18}O$ of surface waters shows a good correlation with the global meteoric water line (GMWL). C) Elevation of the western Andean flank vs. δ^2H. D) Elevation of the eastern Andean flank vs. δ^2H.

in the Malargüe area is solely sourced by the northeasterly wind source.

Another interesting result from our OPI model is that the predicted δ^2H for our sample locations show a well-defined linear relationship between isotopic fractionation and *maximum lifting*, which is defined as the maximum elevation along the path upwind of the sample point (see Brandon et al., 2022b for details). The relationship between precipitation δ^2H and local elevation is also linear, but the quality of the fit is weaker. One could use local elevation, but it is likely that this relationship is simply due to the fact that local elevation will always show a correlation with maximum lifting. Maximum lifting is viewed as a better descriptive variable given that it has a more direct tie to the process of orographic lifting.

Fig. 7 shows that the isotopic composition of the moisture that reaches Malargüe is fractionated along its wind path as it crosses two basement highs of the southern Sierras Pampeanas (sierras de Córdoba and San Luis) and the lower eastern flank of the SCA. This lifting produces precipitation and isotopic fractionation over an 800 km path upwind of Malargüe. The modern precipitation that falls at Malargüe is highly depleted, with an estimated δ^2H of −91.5‰ (Fig. 7C). Thus, isotopic fractionation observed at the stratigraphic section in the Malargüe basin provides a record of the topography upwind of that location, rather than simply the elevation of the Malargüe basin or the height of the Andes.

3.2. Cenozoic record of water δ^2H

δ^2H analyses of volcanic glass are used to calculate the isotopic composition of meteoric precipitation reaching Malargüe over the time span Eocene to present. Estimated water δ^2H values are shown (Fig. 8) as red dots with errors bars (± 1 SE, analytical error). The variation from point to point along the record is like that expected for the estimated analytical errors, which suggests that natural variation at the time scale of the sampling interval (∼0.4 Ma) is smaller than the analytical variation.

The opiPredict program provides an estimate of how variations in climate would influence the isotopic composition of orographic precipitation. We have found that sea-level surface-air temperature, T_0, has the strongest effect, and other climate variables, such as wind speed, wind direction, and buoyant stability, have little influence. This temperature sensitivity affects isotopic composition in two ways. The first is associated with base precipitation, which is defined as the precipitation that would occur if there were no topography (Brandon, 2022). The isotopic composition of this component of the precipitation will be heavier as temperature increases (e.g., Fig. 3 in Dansgaard, 1964). The second is the isotopic lapse rate. The OPI model shows that this rate decreases with increasing T_0. Here we lay out a method that corrects for these two temperature sensitivities, and provides an estimate of the average T_0 in a study area as a function of latitude and age. South America has not rotated or changed latitude appreciably (Müller et al., 2016). Plate reconstructions indicate that the paleolatitude of the Malargüe region has not changed significantly (∼1°) since the Eocene.

We propose the following scaling approximation for estimating the isotopic composition of base precipitation at a specified location and age,

$$\delta^2H_{0,past} = \delta^2H_{0,present} + s_{base}(T_{0,past} - T_{0,present}) + \left(\delta^2H_{sw,past} - \delta^2H_{sw,present}\right)$$

where $\delta^2H_{0,present}$ is the isotopic composition of the present base precipitation (known from the OPI solution), $T_{0,present}$ and $T_{0,past}$ are the present and past sea-level surface-air temperature, and

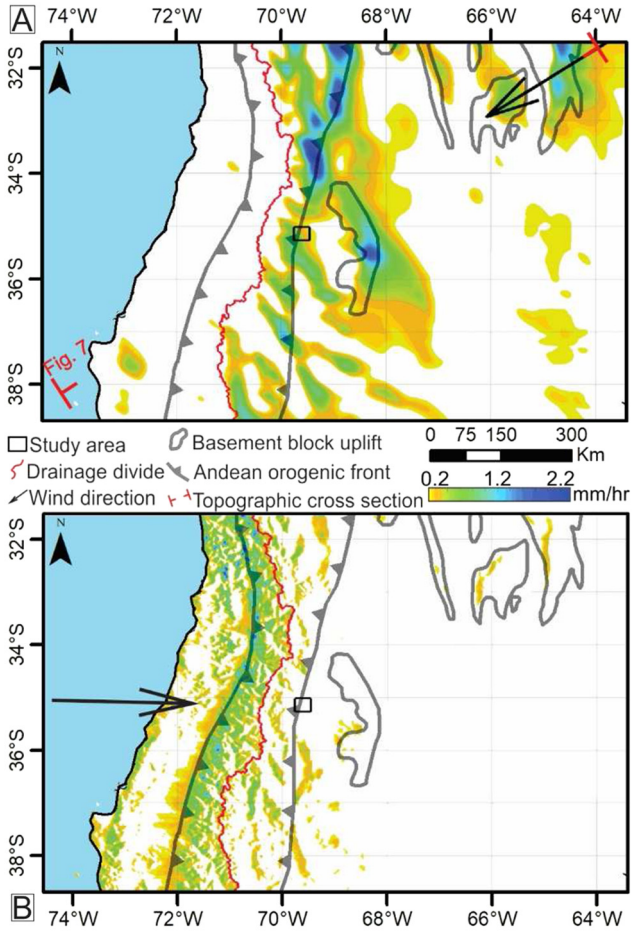

Fig. 6. Maps of predicted orographic precipitation rate for the best-fit solution of the OPI "two-wind" model to the modern meteoric water samples. A) Northeasterly wind source, and B) the Westerly wind source.

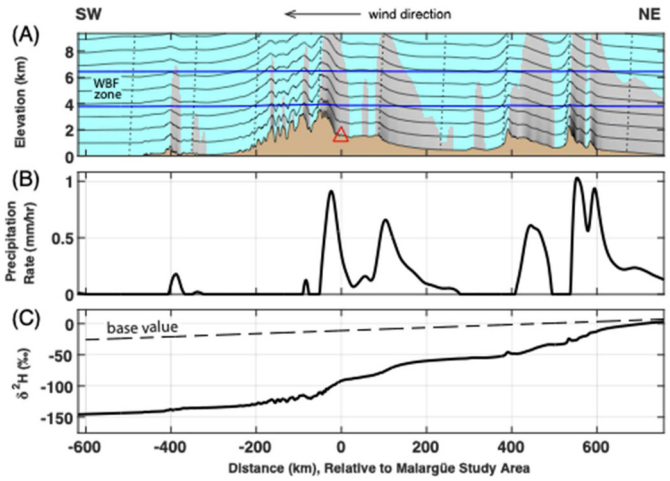

Fig. 7. Cross section of precipitation state caused by northeasterly wind source (see Fig. 6A), as defined by the best-fit solution determined by opiFit_TwoWinds using the modern meteoric water samples. A) Features include the topography (brown), air flow (black streamlines), cloud-water distribution (gray), and precipitation fall lines (dotted black lines). The Wegener-Bergeron-Findeisen (WBF) zone is delimited by the two blue lines, and marks the upward transition in the atmosphere from rain to ice. B) Predicted orographic precipitation. C) Predicted precipitation δ^2H. The dashed line shows the δ^2H composition of base precipitation, which includes an estimated latitudinal gradient.

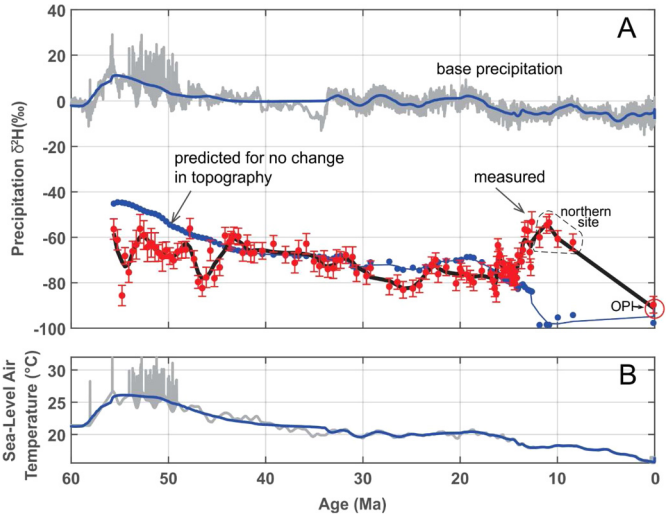

Fig. 8. A) Hydrogen isotopic composition of precipitation as a function of age. The red points show the measured precipitation δ^2H values, and the error bars show the analytical uncertainty at ± 1 SE. The associated black line shows the long-term variation of these measurements (smoothed using LOWESS regression with a 5 Ma span). The blue line with points shows the predicted δ^2H precipitation values after accounting for climate at the sample age but otherwise maintaining the topography the same as modern. The associated blue line shows the long-term variation of this predicted reference case (LOWESS regression, 5 Ma span). The gray line at the top of the plot shows the predicted isotopic composition for base precipitation at the latitude of the samples, after correction for climate. The associated blue line shows the long-term variation (LOWESS regression, 5 Ma span) for this base δ^2H record. B) Predicted sea-level surface-air temperature, T_0, at the latitude of Malargüe and as a function of age. The gray line shows the T_0 record at the ~5.2 ka sampling interval used by Miller et al. (2020) for the Cenozoic benthic foraminifera record. The associated blue line shows the long-term variation (LOWESS regression, 5 Ma span) for this T_0 record.

$\delta^2H_{sw,present}$ and $\delta^2H_{sw,past}$ are the present and past isotopic composition of seawater. The first term on the right side of the equation accounts for the effect of temperature on isotopic fractionation, and the second term on the right accounts for the change with age in the isotopic composition of the oceans. The evolution of δ^2H_{sw} with age is provided by the benthic foraminifera record (e.g., Miller et al., 2020)

The coefficient s_{base} is estimated using the slope of the best-fit line for monthly measurements of δ^2H as a function of the monthly temperature. For our study, we used Mendoza and Ñancuñan GNIP station data, both of which are in the foreland east of the SCA. These data indicate $s_{base} = 2.37$ per mil/°C (Brandon et al., 2022b).

The OPI model is used to calculate the influence of T_0 on isotope fractionation associated with orographic precipitation (i.e., the isotopic lapse rate). This is done by running the OPI model at 1 Ma increments over the duration of the Cenozoic. The parameters T_0 and δ^2H_0 are varied as a function of age, but the topography and the other OPI parameters are maintained at their modern values. Fig. 8b shows the estimated T_0 record for Malargüe. This record was calculated using the Cenozoic benthic foraminifera temperature record (Miller et al., 2020) and a moist energy balance model (MEBM) (Flannery, 1984; Roe et al., 2015; MATLAB code for MEBM provided by Gerard Roe in 2019) to represent changing global temperature with time. Further details are in Brandon et al. (2022b).

The convention at present is to focus on the variation in the measured isotopic composition, and to translate that variation into variations in paleo-elevation using an estimated isotopic lapse rate. Fig. 9 shows a more complete way to relate the δ^2H record, provided by our hydrated glass samples, to changes in maximum lifting with age. We introduce a new variable, the isotope fractionation ratio during lifting, defined by

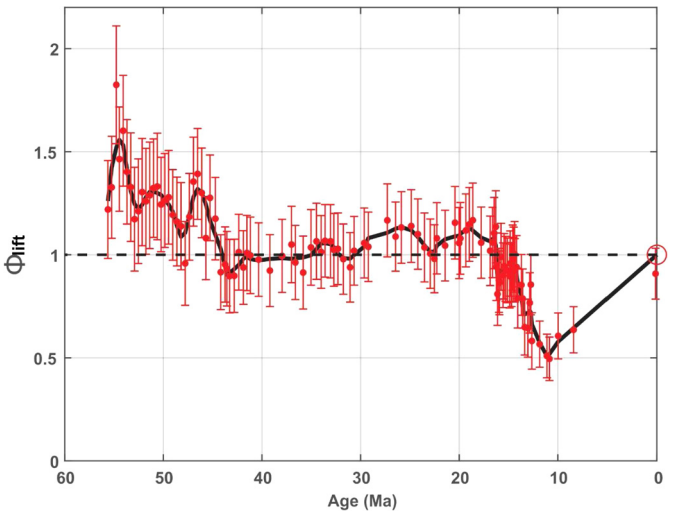

Fig. 9. Predicted evolution of Φ_{lift}, which is the ratio of the observed isotopic fractionation estimated for the sample location and age, relative to predicted isotopic fractionation at the same location and age but for a topography that remains the same as modern. These fractionations have been corrected for have been corrected for climate-related variations in the isotopic lapse rate, and the sea-level air temperature (T_0) with age. The red points show Φ_{lift} for the samples, and the error bars show estimated total uncertainties at ±1 SE. The black line shows the long-term variation of Φ_{lift} (LOWESS regression, 5 Ma span), and the black dashed line marks $\Phi_{\text{lift}} = 1$, which is the prediction for a topography that was the same as the modern topography.

$$\Phi_{\text{lift}} = \frac{\ln(1+\delta^2\text{H}_{\text{past}}) - \ln(1+\delta^2\text{H}_{0,\text{past}})}{\ln(1+\delta^2\text{H}^*_{\text{past}}) - \ln(1+\delta^2\text{H}_{0,\text{past}})} \approx \frac{\delta^2\text{H}_{\text{past}} - \delta^2\text{H}_{0,\text{past}}}{\delta^2\text{H}^*_{\text{past}} - \delta^2\text{H}_{0,\text{past}}}.$$

The central part of this equation gives the exact definition, and the part on the right shows the calculation using the usual delta approximation for logarithms. The variable $\delta^2\text{H}_{\text{past}}$ is the isotopic composition measured for a sample from a specified location and age (e.g., the precipitation δ^2H recorded by hydrated glass). $\delta^2\text{H}_{0,\text{past}}$ is the isotopic composition of the base precipitation at that same location and age. $\delta^2\text{H}^*_{\text{past}}$ is the isotopic composition predicted by OPI for that location and age, but with the topography unchanged relative to present.

In other words, Φ_{lift} is the ratio of the observed isotopic fractionation due to orographic lifting at a specified location and age, relative to the predicted fractionation that would be observed at that age if the past topography were the same as the modern topography. This relationship can be calculated for any point in the landscape. The OPI model shows that there is a linear relationship between isotopic fractionation and maximum lifting. As a result, Φ_{lift} is an approximate measure of the change in upwind topography relative to that for the modern.

For example, if $\Phi_{\text{lift}} < 1$, then we would infer that the orographic fractionation was less than the expected fractionation at that time in the past with a topography equivalent to the present. The conclusion is that the topography was lower in the past relative to the present topography. In turn, if $\Phi_{\text{lift}} > 1$, then the orographic fractionation is greater than that produced at that time in the past with a topography the same at the present topography. The conclusion is that the topography was higher in the past relative to the present topography.

The record of Φ_{lift} shown in Fig. 9 is defined by point measurements (red dots with error bars), and by a smoothed curve (black line), which is meant to emphasize long-period variation in Φ_{lift} and to reduce short-period variation caused by errors. The error bars indicate the estimated uncertainty for Φ_{lift} at the ± 1 standard-error (SE) level. The uncertainty for Φ_{lift} includes the propagated errors for δ^2H of the precipitation and the base-precipitation, and for errors related to registration of the low-precision ages of the samples with the high-resolution age scale for T_0 record (see the opiPredictPlot program in Brandon, 2022 for details). The Φ_{lift} record indicates that from 55 to 45 Ma, the topography upwind of Malargüe was higher, by about 50%, relative to the modern topography along the upwind path. From 45 to 15 Ma, the upwind topography was relatively steady and similar in height to the modern upwind topography. From 15 to 10 Ma, the record shows a 50% drop in the height of the upwind topography. From 10 Ma to present, the upwind topography rose to its modern height. At present, the highest areas along the northeasterly path are Malargüe (1600 m), Sierra de San Luis (1600 m) and Sierra de Córdoba (2500 m). Thus, in our discussion below about the interpretation of these data, we need to consider if the changes in topography are related to the basement highs of the southern Sierras Pampeanas, or to uplift of the Malargüe basin itself.

4. Discussion

When we started our project, we were thinking that δ^2H measurement of volcanic glass from the Malargüe basin would provide information about topographic evolution of the SCA. What we have learned is that the precipitation isotopes preserved in volcanic glass at our sample area are relative to fractionation of water vapor that came out of the northeast. As a result, our record is providing information about the topographic evolution of the foreland and the southern Sierras Pampeanas, and not about the SCA.

We start here with some comments about the influence of climate on precipitation δ^2H, and then conclude with a discussion about possible tectonic interpretations for our Φ_{lift} record.

4.1. Influence of climate on the precipitation δ^2H record

Our δ^2H record (Fig. 8) has information about climate, as well as orographic lifting. Fig. 8 shows that the δ^2H composition of the base precipitation changed from about +10 to −10 per mil over the time interval of 55 Ma to present. This climate-induced change is equivalent to the isotopic fractionation associated with an increase in maximum lifting of about 800 m.

Fig. 8 can be used to estimate the relative magnitude of the isotope lapse rate with time. The isotopic lapse rate is proportional to the offset in the precipitation δ^2H predicted by OPI for no topographic change (blue line with dots), and the base precipitation δ^2H. We find that, for Malargüe, the isotope lapse rate during the Early Eocene was 55% of its modern value. These large variations highlight the need for isotope paleotopography studies to include corrections for climate.

The sampling in the Malargüe section (∼0.4 Ma interval) is dense enough to capture the warm conditions of the Late Paleocene to Early Eocene (∼56 to 48 Ma; Miller et al., 2020). And, in fact, the δ^2H curve shows a positive anomaly over this age interval. There are several short hyperthermal events during this interval, the most familiar being the Paleocene-Eocene Thermal Maximum (PETM), but these events are thought to last for only ∼100 ka, which is short enough to be missed by our sampling. The Early Eocene Climatic Optimum (EECO, 53.4–51.6 Ma) is about 1.8 Ma in duration, and may be represented in our δ^2H record.

We mention these potential correlations not as conclusions, but rather as targets for future study. Our work suggests that it should be possible to develop high resolution time series for precipitation δ^2H in terrestrial settings. This research would also provide useful information about the reliability of volcanic glass to sample meteoric water and to preserve that sample over long geologic intervals.

4.2. Tectonic interpretation for Φ_{lift}

The tectonic interpretation of our results starts with three important conclusions.

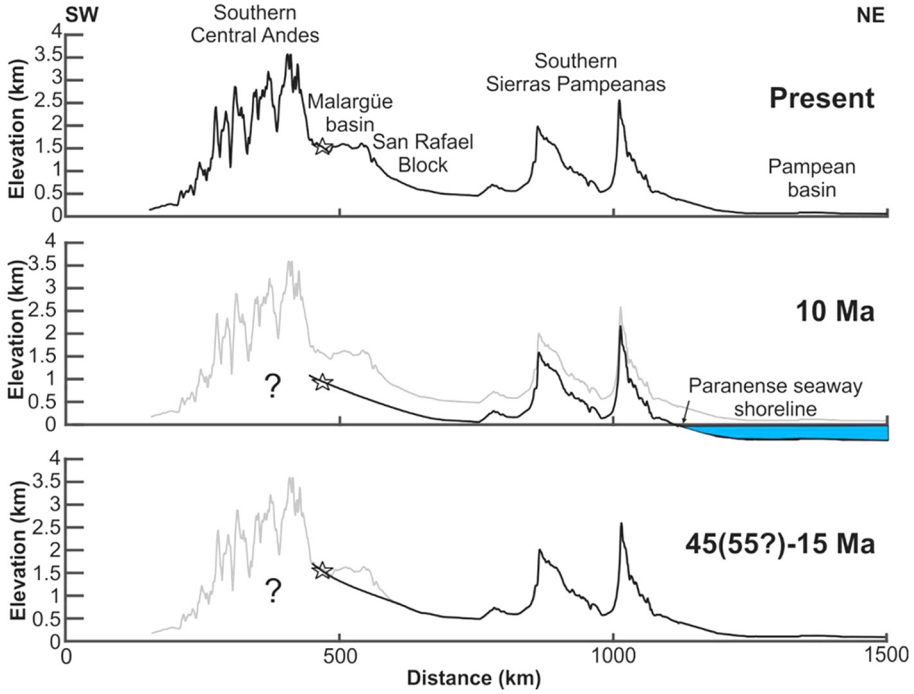

Fig. 10. Schematic representation of the topographic evolution of the Southern Central Andes foreland (unfilled star denotes the position of the Malargüe basin). Our isotopic data and the record provided by the Paranense Seaway indicate that the subsidence/uplift cycle that occurred between 15 and 0 Ma had an amplitude of about 500 m.

1) The precipitation that falls on the east side of the SCA is presently derived almost entirely from moist winds coming out of the northeast. The isotopic fractionation along this wind path occurs by lifting over the Córdoba and San Luis basement highs, and over the eastern foothills of the SCA, just below Malargüe. Westerly moist air can pass over the range, but downslope flow over the east side means that this source becomes strongly undersaturated, so precipitation from this source is suppressed in this area.
2) Our volcanic glass data indicate that the Malargüe area has been receiving precipitation that is strongly depleted, by −50 to −90 per mil for δ^2H, since 55 Ma to present. The only way to produce this depletion is by upslope flow of moist winds and associated precipitation over the eastern side of the range. Thus, we conclude that the high topography of the SCA was formed prior to 55 Ma and has remained high standing from that time to present.
3) If the second conclusion holds, then the first conclusion must extend into the past. In other words, precipitation on the east side of the SCA must have been sourced from moist winds that passed over the basement highs of the Sierras Pampeanas, the foreland, and the SCA foothills. The Malargüe basin was accreted into the SCA thrust belt at about 5 Ma, so the topographic changes recorded by our δ^2H data cannot be attributed to tectonic uplift within the SCA until after 5 Ma. We now focus on the evolution of the Φ_{lift} record.

At ∼55 Ma, topography upwind of Malargüe was 1.5 times higher than at present and then decreased, reaching the same size as present by 45 Ma. The present topography along the northeast upwind path from Malargüe has a maximum elevation of about 2500 meters (Sierra de Córdoba), so we estimate that the topography of the foreland, along with the basement highs, had a maximum height of about 3700 m at 55 Ma.

We recognize that the wind direction may have been different during the Eocene than that for the present. Nonetheless, the hydrated volcanic glass and precipitation δ^2H indicated by that glass require that there be moist winds blowing into the east side of the SCA. The high-standing topography that caused the isotopic fractionation of the water vapor that produced that precipitation had to be somewhere in the foreland region. In our view, Sierra de Córdoba is a reasonable candidate for this early topography. The Φ_{lift} record indicates that the foreland topography remained steady ($\Phi_{\text{lift}} \approx 1$) for the time 45 to 15 Ma (Fig. 10).

The next change is at 15 to 0 Ma, and is marked by a decrease in the upwind topography to 0.5 times the present, and then arriving at the present topography at 0 Ma. The timing of this event coincides with the widespread 15–10 Ma Paranense marine transgression, which floods much of the Pampas and Chaco plains (Fig. 10) (Hernández et al., 2005). While shortening during middle Miocene times has been widely documented (Giambiagi et al., 2008; Turienzo et al., 2012; Horton et al., 2016; Ramos et al., 2014), the subsidence recorded by Neogene foreland deposits has a wavelength of 800 km, which is too large to be related to thrust loading (Dávila et al., 2010; Folguera et al., 2015). Since our isotopic results indicate that the elevation of the Malargüe basin and basement highs topography along its wind path would have all decreased compared to sea level, we think that long-wavelength subduction-induced dynamic topography is a likely explanation. Flament et al. (2015) models have recognized a subsidence and uplift cycle associated with changing subduction geometry and kinematics in the vicinity of Malargüe.

5. Conclusions

Our study shows the viability of using volcanic glass from clastic sedimentary rocks to measure the evolution of topography via the isotope-paleotopography method. Our dense sampling reveals variations in past water isotopes that can be correlated to changes in climate, as well as to changes in topography. We show that much of the observed Eocene to modern orographic isotopic fractionation in the Malargüe basin is probably associated with moist air coming from the northeast, across a path of ∼800 km or longer. As a result, the isotopic signature of precipitation reflects topogra-

phy along this upwind path, and is not due to local elevation or the height of the Andean range. We use an orographic precipitation model to estimate the isotopic composition of base precipitation and the changes in orographic fractionation with time and temperature, and cast these into Φ_{lift} to identify three key Cenozoic topographic events: 1) From 55-45 Ma, the topographic lifting factor, Φ_{lift}, decreases from 1.5 to 1, relative to present topography upwind of Malargüe. Strong fractionation during this warm climate interval requires a high Andes to the west at 55 Ma, and may reflect early growth of the Sierras Pampeanas basement highs to higher than modern. 2) From 45-15 Ma, Φ_{lift} is $\sim$1, indicating a prolonged period of topographic stasis across the foreland and southern Sierras Pampeanas. 3) From 15 to 0 Ma, Φ_{lift} decreases to 0.5 and then back to 1. We attribute the surface lowering to dynamic subsidence as proposed by numerical modeling (Flament et al., 2015). The observed amount of surface lowering is consistent with the 15-10 Ma Paranense marine transgression. Dynamic modeling and marine regression after 10 Ma indicate dynamic rebound to modern foreland elevations.

CRediT authorship contribution statement

Lucas M. Fennell: Conceptualization, Funding acquisition, Investigation, Methodology, Visualization, Writing – original draft. **Mark T. Brandon:** Conceptualization, Funding acquisition, Investigation, Software, Supervision, Visualization, Writing – review & editing. **Michael T. Hren:** Conceptualization, Formal analysis, Funding acquisition, Investigation, Supervision, Writing – review & editing.

Declaration of competing interest

The authors declare that they have no known competing financial interests or personal relationships that could have appeared to influence the work reported in this paper.

Data availability

All data and software used in this work are reported in the paper, the associated Supplementary Materials, and in Brandon (2022) and Brandon et al. (2022a).

Acknowledgements

We acknowledge Federico Martos for his assistance in the field, David Auerbach Colwyn and Amelia Lewis for their assistance in the lab and Andrés Folguera for his invaluable support. We are grateful with Marcelo Farías and an annonymous reviewer for their valuable comments. Both a CONICET Internship Abroad Program for Postdoctoral Fellows and a Fulbright-Ministry of Education Fellowship are acknowledged for my two 3-month research stays in Yale University during 2018 and 2019. This work was funded by National Science Foundation EAR-1650313 and National Science Foundation EAR-1650396 awards to Mark Brandon and Michael Hren, respectively. This is the R-446 contribution of the Instituto de Estudios Andinos "Don Pablo Groeber" (UBA-CONICET).

Appendix A. Supplementary material

Supplementary material related to this article can be found online at https://doi.org/10.1016/j.epsl.2023.117991.

References

Ambach, W., Dansgaard, W., Eisner, H., Møller, J., 1968. The altitude effect on the isotopic composition of precipitation and glacier ice in the Alps. Tellus 20, 595–600. https://doi.org/10.3402/tellusa.v20i4.10040.

Allmendinger, R.W., 1986. Tectonic development, southeastern border of the Puna Plateau, northwestern Argentine Andes. Geol. Soc. Am. Bull. 97, 1070–1082. https://doi.org/10.1130/0016-7606(1986)97<1070:TDSBOT>2.0.CO;2.

Blisniuk, P., Stern, L.A., 2005. Stable isotope paleoaltimetry: a critical review. Am. J. Sci. 305, 1033–1074. https://doi.org/10.2475/ajs.305.10.1033.

Brandon, M.T., 2022. MATLAB Programs for the analysis of orographic precipitation and isotopes (OPI), with implications for the study of paleotopography (OPI 3.6) [Software]. Zenodo. https://doi.org/10.5281/zenodo.7076557. https://github.com/foret37/OPI-Orographic-Precipitation-and-Isotopes/tree/v3.6.002, 2022.

Brandon, M.T., Chang, Q., Hren, M.T., 2022a. Analysis of Orographic Precipitation and Isotopes in the Vicinity of the Patagonian Andes (Latitude 54.8 to 40.1 S) (OPI-Patagonia_v1.001) (OPI-Patagonia_v1.001) [Data set], Zenodo. https://github.com/foret37/OPI-Patagonian-Andes/tree/OPI-Patagonia_v1.001.

Brandon, M.T., Fennell, L.M., Hren, M.T., 2022b. Analysis of orographic precipitation and isotopes in the vicinity of the South-Central Andes (latitude 37.6 to 32.4 S) (OPI-SCA 1.0.000) [Data set]. Zenodo. https://doi.org/10.5281/zenodo.7077455. https://github.com/foret37/OPI-South-Central-Andes/tree/OPI-SCA_v1.0.002.

Cassel, E.J., Breecker, D.O., 2017. Long-term stability of hydrogen isotope ratios in hydrated volcanic glass. Geochim. Cosmochim. Acta 200, 67–86. https://doi.org/10.1016/j.gca.2016.12.001.

Cerling, T.E., Brown, F.H., Bowman, J.R., 1985. Low-temperature alteration of volcanic glass: hydration, Na, K 18O and Ar mobility. Chem. Geol., Isot. Geosci. Sect. 52, 281–293. https://doi.org/10.1016/0168-9622(85)90040-5.

Combina, A.M., Nullo, F., 2011. Ciclos tectónicos, volcánicos y sedimentarios del Cenozoico del sur de Mendoza-Argentina (35°-37°S y 69°30'W). Andean Geol. 38, 198–218.

Combina, A.M., Nullo, F., 1997. Consideraciones tectosedimentarias sobre la formación Río Diamante, Cordillera de los Andes, Argentina. Cuad. Geogr. Ibér. 22, 305–320. https://doi.org/10.5209/rev_CGIB.1997.v22.2511.

Colwyn, D.A., Brandon, M.T., Hren, M.T., Hourigan, J., Pacini, A., Cosgrove, M.G., Midzik, M., Garreaud, R.D., Metzger, C., 2019. Growth and steady state of the Patagonian Andes. Am. J. Sci. 319, 431–472. https://doi.org/10.2475/06.2019.01.

Dansgaard, W., 1964. Stable isotopes in precipitation. Tellus 16, 436–468. https://doi.org/10.1111/j.2153-3490.1964.tb00181.x.

Dávila, F.M., Lithgow-Bertelloni, C., Giménez, M., 2010. Tectonic and dynamic controls on the topography and subsidence of the Argentine Pampas: the role of the flat slab. Earth Planet. Sci. Lett. 295, 187–194. https://doi.org/10.1016/j.epsl.2010.03.039.

Drummond, C.N., Wilkinson, B.H., Lohmann, K.C., Smith, G.R., 1993. Effect of regional topography and hydrology on the lacustrine isotopic record of Miocene paleoclimate in the Rocky Mountains. Palaeogeogr. Palaeoclimatol. Palaeoecol. 101, 67–79.

Farías, M., Comte, D., Charrier, R., Martinod, J., David, C., Tassara, A., Tapia, F., Fock, A., 2010. Crustal-scale structural architecture in central Chile based on seismicity and surface geology: implications for Andean mountain building. Tectonics 29, TC3006. https://doi.org/10.1029/2009TC002480.

Fick, S.E., Hijmans, R.J., 2017. WorldClim 2: new 1-km spatial resolution climate surfaces for global land areas. Int. J. Climatol. 37 (12), 4302–4315. https://doi.org/10.1002/joc.5086.

Flament, N., Gurnis, M., Müller, R.D., Bower, D.J., Husson, L., 2015. Influence of subduction history on South American topography. Earth Planet. Sci. Lett. 430, 9–18. https://doi.org/10.1016/j.epsl.2015.08.006.

Flannery, B.P., 1984. Energy balance models incorporating transport of thermal and latent energy. J. Atmos. Sci. 41, 414–421. https://doi.org/10.1175/1520-0469(1984)041<0414:EBMITO>2.0.CO;2.

Folguera, A., Zárate, M., Tedesco, A., Dávila, F., Ramos, V.A., 2015. Evolution of the Neogene Andean foreland basins of the Southern Pampas and Northern Patagonia (34°-41°S), Argentina. J. South Am. Earth Sci. 64, 452–466. https://doi.org/10.1016/j.jsames.2015.05.010.

Folguera, A., Zárate, M., 2019. Late oligocene to quaternary tectonic evolution of the extra Andean basins of the pampean plain, Argentina. J. South Am. Earth Sci. 94, 102207. https://doi.org/10.1016/j.jsames.2019.05.023.

Friedman, I., Gleason, J., Sheppard, R.A., Gude, A.J., 1993a. Deuterium Fractionation as Water Diffuses into Silicic Volcanic Ash. Geophysical Monograph Series, vol. 78, pp. 321–323.

Friedman, I., Gleason, J., Warden, A., 1993b. Ancient Climate from Deuterium Content of Water in Volcanic Glass. Geophysical Monograph Series, vol. 78, pp. 309–319.

Garrido, A., Kramarz, A., Forasiepi, A., Bond, M., 2012. Estratigrafía, mamíferos fósiles y edad de las secuencias volcanosedimentarias eoceno-miocenas de la sierra de Huantraico-sierra Negra y cerro Villegas (provincia del Neuquén, Argentina). Andean Geol. 39, 482–510. https://doi.org/10.5027/andgeoV39n3-a07.

Garzione, C.N., Dettman, D.L., Quade, J., DeCelles, P.G., Butler, R.F., 2000. High times on the Tibetan Plateau: paleoelevation of the Thakkhola graben, Nepal. Geology 28, 339–342.

Giambiagi, L.B., Bechis, F., García, V.H., Clark, A.H., 2008. Temporal and spatial relationships of thick- and thin-skinned deformation: a case study from the Malargüe fold-and-thrust belt, southern Central Andes. Tectonophysics 459, 123–139. https://doi.org/10.1016/j.tecto.2007.11.069.

Hernández, R.M., Jordan, T.E., Dalenz Farjat, A., Echavarría, L., Idleman, B.D., Reynolds, J.H., 2005. Age, distribution, tectonics, and eustatic controls of the

Paranense and Caribbean marine transgressions in southern Bolivia and Argentina. J. South Am. Earth Sci. 19, 495–512. https://doi.org/10.1016/j.jsames.2005.06.007.

Hildreth, W., Godoy, E., Fierstein, J., Singer, B., 2009. Laguna del Maule Volcanic Field: eruptive history of a quaternary basalt-to-rhyolite distributed volcanic field on the Andean range crest in central Chile. Bol. Serv. Nac. Geol. Min. 63. 143 p.

Hildreth, W., Grunder, A.L., Drake, R.E., 1984. The Loma Seca Tuff and the Calabozos caldera: a major ash-flow and caldera complex in the southern Andes of central Chile. Geol. Soc. Am. Bull. 95, 45–54.

Horton, B.K., 2018. Sedimentary record of Andean mountain building. Earth-Sci. Rev. 178, 279–309. https://doi.org/10.1016/j.earscirev.2017.11.025.

Horton, B.K., Fuentes, F., 2016. Sedimentary record of plate coupling and decoupling during growth of the Andes. Geology 44, 647–650. https://doi.org/10.1130/G37918.1.

Horton, B.K., Fuentes, F., Boll, A., Starck, D., Ramirez, S.G., Stockli, D.F., 2016. Andean stratigraphic record of the transition from backarc extension to orogenic shortening: a case study from the northern Neuquén Basin, Argentina. J. South Am. Earth Sci. 71, 17–40. https://doi.org/10.1016/j.jsames.2016.06.003.

Kay, R.W., Mahlburg-Kay, S., 1991. Creation and destruction of lower continental crust. Geol. Rundsch. 80, 259–278. https://doi.org/10.1007/BF01829365.

Litvak, V.D., Fernández Paz, L., Iannelli, S., Poma, S., Folguera, A., 2019. Cenozoic arc-related magmatism in the southern Central and North Patagonian Andes. In: Andean Tectonics. Elsevier, pp. 573–607.

Miller, K.G., Browning, J.V., Schmelz, W.J., Kopp, R.E., Mountain, G.S., Wright, J.D., 2020. Cenozoic sea-level and cryospheric evolution from deep-sea geochemical and continental margin records. Sci. Adv. 6 (20), eaaz1346. https://doi.org/10.1126/sciadv.aaz1346.

Müller, R.D., Seton, M., Zahirovic, S., Williams, S.E., Matthews, K.J., Wright, N.M., Shephard, G.E., Maloney, K.T., Barnett-Moore, N., Hosseinpour, M., Bower, D.J., Cannon, J., 2016. Ocean basin evolution and global-scale plate reorganization events since Pangea breakup. Annu. Rev. Earth Planet. Sci. 44, 107–138. https://doi.org/10.1146/annurev-earth-060115-012211.

Norris, R.D., Corfield, R.M., Hayes-Baker, K., 1999. Mountains and Eocene climate. In: Warm Climates in Earth History. Cambridge University Press, pp. 161–196.

Poage, M.A., Chamberlain, C.P., 2001. Empirical relationships between elevation and the stable isotope composition of precipitation and surface waters: considerations for studies of paleoelevation change. Am. J. Sci. 301, 1–15. https://doi.org/10.2475/ajs.301.1.1.

Ramos, V.A., 1999. Plate tectonic setting of the Andean Cordillera. Episodes 22 (3), 183–190. https://doi.org/10.18814/epiiugs/1999/v22i3/005.

Ramos, V.A., Litvak, V.D., Folguera, A., Spagnuolo, M., 2014. An Andean tectonic cycle: from crustal thickening to extension in a thin crust (34°-37°SL). Geosci. Front. 5, 351–367. https://doi.org/10.1016/j.gsf.2013.12.009.

Roe, G.H., Feldl, N., Armour, K.C., Hwang, Y.T., Frierson, D.M.W., 2015. The remote impacts of climate feedbacks on regional climate predictability. Nat. Geosci. 8, 135–139. https://doi.org/10.1038/ngeo2346.

Rowley, D.B., Pierrehumbert, R.T., Currie, B.S., 2001. A new approach to stable isotope-based paleoaltimetry: implications for paleoaltimetry and paleohypsometry of the High Himalaya since the Late Miocene. Earth Planet. Sci. Lett. 5836, 1–17. https://doi.org/10.1016/S0012-821X(01)00324-7.

Rowley, D.B., Garzione, C.N., 2007. Stable isotope-based paleoaltimetry. Annu. Rev. Earth Planet. Sci. 35, 463–508. https://doi.org/10.1146/annurev.earth.35.031306.140155.

Stern, C., Amini, H., Charrier, R., Hervé, F., Varela Barbagelata, J., Godoy, E., 1984. Petrochemistry and age of rhyolitic pyroclastic flows which occur along the drainage valleys of the rio Maipo and río Cachapoal (Chile) and the río Yaucha and río Papagayos (Argentina). Rev. Geol. Chile 23, 39–52.

Strecker, M.R., Alonso, R.N., Bookhagen, B., Carrapa, B., Hilley, G.E., Sobel, E.R., Trauth, M.H., 2007. Tectonics and climate of the southern central Andes. Annu. Rev. Earth Planet. Sci. 35, 747–787. https://doi.org/10.1146/annurev.earth.35.031306.140158.

Turienzo, M.M., Dimieri, L.v., Frisicale, M.C., Araujo, V., Sánchez, N., 2012. Cenozoic structural evolution of the Argentinean Andes at 34°30'S: a close relationship between thick and thin-skinned deformation. Andean Geol. 39, 317–357.

Upton, G.J., 2008. A Dictionary of Statistics, 2nd edition. Oxford University Press, eISBN: 9780191726866, the formula for the pooled estimate of the standard deviation is reported in the entry: "Pooled estimate of common mean".